^2H NMR Study of Lattice Dynamics Affecting the Rate of Intramolecular Electron Transfer in Mixed-Valence $[Fe_3O(O_2CCH_3)_6(py)_3](py)$

Scott E. Woehler,[1] Richard J. Wittebort,*[1] Seung M. Oh,[2] Takeshi Kambara,[2,3] David N. Hendrickson,*[2] Daryl Inniss,[4] and Charles E. Strouse*[4]

Contribution from the Department of Chemistry, University of Louisville, Louisville, Kentucky 40292, the School of Chemical Sciences, University of Illinois, Urbana, Illinois 61801, and the Department of Chemistry and Biochemistry, University of California, Los Angeles, California 90024. *Received May 1, 1986*

Abstract: Intramolecular electron transfer in the mixed-valence complex $[Fe_3O(O_2CCH_3)_6(py)_3](py)$, where py is pyridine, is investigated in the solid state. Phase transitions and the relationship between the phase transitions and the rate of intramolecular electron transfer are studied. The complex crystallizes in the rhombohedral space group $R32$; a = 17.563 (5) Å and c = 10.853 (3) Å at 200 K and Z = 3. The final discrepancy factors are R = 0.082 and R_w = 0.097 for 935 reflections with $I > 3\sigma(I)$. Fe_3O molecules and disordered pyridine solvate molecules are stacked in alternate sites of 32 symmetry along the threefold (i.e., c) axis. The unit cell contains three such stacks related by a 3_1 axis. The pyridine–pyridine *inter*molecular separation, $c/3$ = 3.6 Å, along the 3_1 axes controls the size of the solvate cavity along the threefold axis. The large thermal parameters observed for the pyridine solvate at 200 K are consistent with a dynamic disorder of this molecule. Two doublets of area ratio 2:1 (Fe^{III}:Fe^{II}) are present in the Mössbauer spectra below ~110 K. As the sample temperature is increased, the spectrum changes to become a single average-valence doublet at temperatures above ~190 K. Four phase transitions (111.4, 112.0, 185.8, and 191.3 K) have been detected in the heat-capacity data for this complex. Changes are seen in the Mössbauer spectra that correspond to these phase transitions. Above the temperature of the two low-temperature phase transition points (111–112 K) a third doublet appears in the Mössbauer spectrum in addition to the Fe^{II} and Fe^{III} doublets seen at lower temperatures. This third doublet has the parameters of an average-valence state. Near the temperature of the two high-temperature phase transitions (186–192 K), the Mössbauer spectrum completes the conversion to this average-valence doublet. The low-temperature phase transitions are assigned to an order–disorder phase transition wherein electronically localized Fe_3O complexes make a transition from a state where there is ordering in the sense of distortion to a state where there is a random disorder in the sense of distortion. The appearance of the average-valence Mössbauer doublet at 111–112 K reflects the fact that the ground-state potential-energy surface for each Fe_3O complex changes at this phase transition. As a consequence there are Fe_3O complexes in the undistorted (i.e., average-valence) state in addition to the three valence-trapped vibronic states. The two high-temperature phase transitions, one of which starts at ~112 K and culminates at ~192 K, are assigned to a combination of the onset of dynamical motion for the pyridine solvate molecules and an increasing rate of *intra*molecular electron transfer in the Fe_3O complexes across the temperature region. The nature of the dymamical motion of the pyridine solvate molecules was studied with solid-state ^2H NMR spectroscopy. Small crystallites of the complex orient in a magnetic field. A collection of magnetically oriented single crystals embedded in a wax block was studied by single-crystal techniques. The easy axis of the magnetic susceptibility tensor (i.e., axis of orientation in a magnetic field) was established to be the c axis of the crystals (C_3 axis). Variable-temperature ^2H NMR studies were carried out for single-crystal collections of $[Fe_3O(O_2CCD_3)_6(C_5H_5N)_3](C_5H_5N)$ and $[Fe_3O(O_2CCH_3)_6(C_5D_5N)_3](C_5D_5N)$. In the first case it was possible to study the electronic localization in the Fe_3O complexes. In the second case the pyridine–solvate dynamics were examined to show that at ~190 K there is an onset of rotation of the solvate molecules about the C_3 axis.

It was reported in previous papers[5-10] that the solid-state environment is a crucial factor in determining the rate of *intra*molecular electron transfer in trinuclear, mixed-valence, iron–acetate complexes of general composite $[Fe_3O(O_2CCH_3)_6(L)_3]\cdot S$, where L is a ligand such as pyridine or substituted pyridines and S is a solvate molecule such as pyridine, benzene, $CHCl_3$, or CH_3CN. The *intra*molecular electron-transfer rate in these mixed-valence complexes is dramatically affected by changing the solvate molecule in the solid state.[5] This solvate-dependent electron-transfer property is attributed to the fact that Fe_3O complexes can have a different crystal packing arrangement depending on the solvate molecule. A crystalline system having a more symmetric lattice (i.e., approaching C_3 site symmetry for the Fe_3O complex) shows a greater electron-transfer rate than those with low symmetry. Change in the crystal environment about a given Fe_3O complex leads to a change in the ground-state potential-energy surface for electron transfer. This influences the rate of *intra*molecular electron transfer, whether the electron transfer occurs by thermal activation and/or quantum mechanical tunneling.

Structural dynamics associated with the ligand and solvate molecules can also influence the rate of intramolecular electron transfer in these systems. Phase transitions associated with the onset of ligand and solvate motion have been detected in heat capacity measurements,[6b,10] multiple-temperature structural analyses,[5,6a] and magnetic resonance observations.[6a,7,8] In many cases these changes are accompanied by changes in the electron-transfer characteristics as reflected in the Mössbauer spectra. In $[Fe_3O(O_2CCH_3)_6(4\text{-Me-py})_3](C_6H_6)$ dynamical motion of the benzene solvate molecule has been definitively established by a single-crystal ^2H study.[7,8] Two-phase transitions (~181 and ~282 K) have been detected for $[Fe_3O(O_2CCH_3)_6(3\text{-Me-py})_3](3\text{-Me-py})$ with heat-capacity measurements.[6b] It is very likely that the onset of a dynamical disorder in the 3-Me-py solvate molecules is occurring in the phase transition at ~282 K. The results of a ^2H

(1) University of Louisville.
(2) University of Illinois.
(3) On sabbatical leave from the Department of Engineering Physics, The University of Electro-Communications, Chofu, Tokyo 183, Japan.
(4) University of California.
(5) (a) Oh, S. M.; Hendrickson, D. N.; Hassett, K. L.; Davis, R. E. *J. Am. Chem. Soc.* **1984**, *106*, 7984. (b) Oh, S. M.; Hendrickson, D. N.; Hassett, K. L.; Davis, R. E. *J. Am. Chem. Soc.* **1985**, *107*, 8009.
(6) (a) Oh, S. M.; Wilson, S. R.; Hendrickson, D. N.; Woehler, S. E.; Wittebort, R. J.; Strouse, C. E. *J. Am. Chem. Soc.*, in press. (b) Sorai, M.; Shiomi, Y.; Hendrickson, D. N.; Oh, S. M. *Inorg. Chem.*, in press.
(7) Oh, S. M.; Kambara, T.; Hendrickson, D. N.; sorai, M.; Kaji, K.; Woehler, S. E.; Wittebort, R. J. *J. Am. Chem. Soc.* **1985**, *107*, 5540.
(8) Woehler, S. E.; Wittebort, R. J.; Oh, S. M.; Hendrickson, D. N.; Inniss, D.; Strouse, C. E. *J. Am. Chem. Soc.* **1986**, *108*, 2938.
(9) Hendrickson, D. N.; Oh, S. M.; Dong, T.-Y.; Kambara, T.; Cohn, M. J.; Moore, M. F. *Comments Inorg. Chem.* **1985**, *4*, 329-349.
(10) Sorai, M.; Kaji, K.; Hendrickson, D. N.; Oh, S. M. *J. Am. Chem. Soc.* **1986**, *108*, 702.

0002-7863/87/1509-1063$01.50/0

NMR study[6a] of the isostructural toluene solvate confirm this.

Interactions between neighboring Fe_3O complexes can result in cooperative behavior that leads to structural phase transitions. This cooperativity can be viewed as arising either electronically through the asymmetries in the charge distributions of neighboring molecules or sterically through the associated structural asymmetry. Temperature dependence in the observed structural asymmetry has been demonstrated in $[Fe_3O(O_2CCH_3)_6(4\text{-Et-py})_3](4\text{-Et-py})$[5] where the Fe_3O triangular framework changes from isosceles to more equilateral with increasing temperature. Dynamic factors may also influence the electron-transfer rate in this complex; onset of dynamic disorder of a 4-Et-py ligand could be associated with a change in the electron-transfer characteristics.

The most detailed results concerning the interrelationships among lattice motion, structural-phase transitions, and intramolecular electron transfer are becoming available for $[Fe_3O(O_2CCH_3)_6(py)_3](py)$. Heat-capacity and preliminary ^{57}Fe Mössbauer results for this complex have been previously reported.[7,10] Phase transitions in the neighborhood of 111–112 and 185–191 K were detected in the heat-capacity data. Changes are seen in the Mössbauer spectrum of this compound at these temperatures. In this paper the single-crystal X-ray structure and the details of the variable-temperature Mössbauer spectroscopy of $[Fe_3O(O_2CCH_3)_6(py)_3](py)$ are presented. In addition, the results of detailed ^2H NMR experiments are presented to probe the electronic localization–delocalization phase transition and the pyridine solvate dynamics. Variable-temperature and single-crystal ^2H NMR results are presented for samples where the acetate ligands are deuterated as well as for samples where all of the pyridines are deuterated.

Experimental Section

Compound Preparation. Pyridine was dried by refluxing over BaO and fractionally distilled under an argon atmosphere. The deuterated chemicals, such as pyridine-d_5 (99.5 atom % D), acetic acid-d_4 (99.5 atom % D), sodium acetate-d_3 (99 atom % D), and deuterium oxide (99.8 atom % D), were purchased from Aldrich Chemical Co. and were used without further purification. Elemental analyses were performed in the Microanalytical Laboratory of the School of Chemical Sciences, University of Illinois.

Samples of $[Fe_3O(O_2CCH_3)_6(py)_3](py)$ were prepared as previously described.[8,11] $[Fe_3O(O_2CCH_3)_6(H_2O)_3]$ (5 g, 8.4 mmol) was dissolved in ~30 mL of pyridine under an argon atmosphere. The reaction mixture was stirred for 1 h at 50–60 °C. A small amount of insoluble solid was filtered off. The mixture was then cooled to room temperature and stored for 3 days in a glovebox. Slow evaporation of the solvent produced a black crystalline product which was filtered and dried briefly under vacuum [yield was 5.6 g (78%)]. Anal. Calcd for $C_{32}Fe_3H_{38}N_4O_{13}$: C, 44.99; Fe, 19.61; H, 4.49; N, 6.56. Found: C, 45.00; Fe, 19.58; H, 4.34; N, 6.32. Crystals suitable for X-ray crystallography were prepared by a recrystallization from pyridine. The crystalline samples of $[Fe_3O(O_2CCD_3)_6(py)_3](py)$ and $[Fe_3O(O_2CCH_3)_6(C_5D_5N)_3](C_5D_5N)$ were prepared by the same method with the corresponding deuterated reagents.

Experimental Methods. Mössbauer data were collected on a previously described apparatus.[12] The Mössbauer data were computer fit to Lorentzian line shapes with the use of a previously described program.[13] The isomer shift values are reported relative to iron foil at 298 K but are not corrected for the temperature-dependent second-order Doppler shift.

^2H NMR experiments were performed on a 5.9 T spectrometer described elsewhere[14,15] with the pulse sequence $[(90)_x\text{–}t/2\text{–}(180)_y\text{–}t/2\text{–}(90)_y\text{–}t/2\text{–}(180)_y\text{–}t/2\text{–observe}]$, which refocuses both the quadrupolar and paramagnetic couplings.[16] A value of $t = 35$ μs was used.

Table I. Crystallographic Data

formula	$[Fe_3O(O_2CCH_3)_6(py)_3](py)$
cryst dimens, mm	0.30 × 0.35 × 0.20
space group	$R32$
a, Å	17.563 (5)
b, Å	17.563 (5)
c, Å	10.853 (3)
volume, Å^3	2915 (1)
density (calcd), g/cm^3	1.47
radiation, Å	Mo, 0.7107
temp, K	200 (2)
scan rate, deg/min	3
scan mode	θ–2θ
2θ mx, deg	50
total reflcns	1258
total reflcns ($I > 3\sigma I$)	935
R	0.082
R_w	0.097
EOF	2.76
no. of parameters refined	73

NMR samples consisted of ~50 mg of microcrystals suspended in hydrocarbon matrix and oriented in the magnetic field. In the case of the single-crystal work, a crystal ~1 mm on each edge was oriented in the magnetic field in a hydrocarbon matrix. That is, the single crystal was suspended in fluid hexadecane (mp = 291 K) and the crystal was then oriented by the 5.9-T field such that the principal axis of the magnetic susceptibility tensor of the crystal is aligned with the magnetic field. The hydrocarbon was then cooled to form a block with the crystal embedded in it. The hydrocarbon block was mounted and rotated about a single axis perpendicular to the magnetic field.

X-Ray Diffraction Characterization of $[Fe_3O(O_2CCH_3)_6(py)_3](py)$. Preliminary examination and data collection were carried out at UCLA with a locally automated Huber diffractometer equipped with a closed cycle low-temperature device. Examination at room temperature established a three-molecule unit cell, space group $R32$. Intensity measurements of three threefold related reflections as a function of temperature revealed a phase change below 200 K. Below the transition temperature a random pattern of peak splitting in the ω scans indicated the presence of twinning, presumably associated with the loss of threefold crystallographic symmetry. This transformation was found to be completely reversible in that warming the crystal above 200 K caused the splitting to disappear and cooling it again produced the same splitting pattern observed previously. There was no obvious relationship between the observed splittings for threefold related reflections.

A single crystal with dimensions 0.30 × 0.35 × 0.20 mm was used for data collection and cell constant determination at 200 K. Least-squares refinement of the settings of 15 automatically centered reflections with $10° < 2\theta < 20°$ led to the cell constants reported in Table I. Experimental crystallographic parameters are summarized in Table I. Three reflections monitored after every 97 reflections showed no significant variation in intensity. Intensities were derived from an analysis of scan profiles.[17] The data were corrected for Lorentz and polarization effects.

Structure Solution and Refinement. Direct methods (MULTAN) were used to solve the structure in the space group $R32$. The unique nonhydrogen atoms were located by successive cycles of full-matrix least-squares refinement and difference Fourier synthesis. The disordered solvate molecule was modeled as a rigid group (C–C = C–N = 1.39 Å, C–H = 1.00 Å) with the nitrogen atoms located on the threefold axis.

Hydrogen atoms were included as fixed contributors to the final refinement cycles. One hydrogen atom for the methyl group was found in an electron density difference map. The other methyl hydrogen atoms were calculated on the basis of idealized geometry (sp^3) and bond length

(11) (a) Wrobleski, J. T.; Dziobkowski, C. T.; Brown, D. B. *Inorg. Chem.* **1981**, *20*, 684. (b) Johnson, M. K.; Cannon, R. D.; Powell, D. B. *Spectrochim. Acta* **1982**, *38A*, 307.

(12) Cohn, M. J.; Timken, M. D.; Hendrickson, D. N. *J. Am. Chem. Soc.* **1984**, *106*, 6683.

(13) Chrisman, B. L.; Tumolillo, T. A. *Comput. Phys. Commun.* **1971**, *2*, 322.

(14) Wittebort, R. J.; Subramanian, R.; Kulshreshtha, N. P.; DuPre, D. B. *J. Chem. Phys.* **1985**, *83*, 2457.

(15) Woehler, S. E.; Wittebort, R. J. *Magn. Reson.*, submitted for publication.

(16) Siminovitch, D. J.; Rance, M.; Jeffries, K. R.; Brown, M. F. *J. Magn. Reson.* **1984**, *58*, 62.

(17) The programs used in this work included modified versions of the following programs: CARESS (Broach, Coppens, Becker, and Blessing), peak profile analysis, Lorentz and polarizaton corrections; MULTAN (Main), package of programs, including direct methods, structure factor normalization, Fourier transform, and peak search; ORFLS (Busing, Martin, and Levy), structure factor calculation and full-matrix least-squares reinfement; ORFFE (Busing, Martin, and Levy), distance, angle, and error calculations; ABSORB (Coppens, Edwards, and Hamilton), absorption correction calculation; ORTEP (Johnson) figure plotting; HYDROGEN (Trueblood), calculation of hydrogen atomic positions. All least-squares refinements computed the agreement factors R and R_w: $R = \sum||F_o| - |F_c||/\sum|F_o|$ and $R_w = [\sum w_i||F_o| - |F_c||^2/\sum w_i|F_o|^2]^{1/2}$ where F_o and F_c are the observed and calculated structure factors, respectively, and $w_i^{1/2} = 1/\sigma(F_o)$. The estimated standard deviation in the integrated intensity, σ_I, was calculated as $(\sigma_I^2(CS) + 0.04I^2)^{1/2}$ where $\sigma(CS)$ is based on counting statistics. The parameter minimized in all least-squares refinements was $\sum w_i||F_o| - |F_c||^2$. All calculations were performed on a DEC VAX 11/750 computer.

Table II. Positional Parameters for $[Fe_3O(O_2CCH_3)_6(py)_3](py)$ at 200 K[a]

atom	x/a	y/b	z/c
Fe	0.1087 (1)	0.0000	0.0000
O(1)	0.0755 (5)	−0.0926 (5)	0.1374 (7)
O(2)	−0.0708 (5)	−0.1705 (5)	0.1294 (7)
C(1)	0.0029 (7)	−0.1535 (8)	0.1681 (11)
C(2)	0.0030 (10)	−0.2163 (12)	0.2641 (16)
N(10)	0.2348 (7)	0.0000	0.0000
C(11)	0.3131 (8)	−0.0780 (9)	−0.0164 (12)
C(12)	0.2371 (8)	−0.0752 (8)	−0.0133 (11)
C(13)	0.3911 (11)	0.0000	0.0000
O	0.0000	0.0000	0.0000
H(11A)	0.3136	−0.1357	−0.0330
H(12A)	0.1791	−0.1325	−0.0201
H(13A)	0.4583	0.0328	0.0073
H(2)	0.0640	−0.2075	0.2767
H(2A)	−0.0353	−0.2790	0.2336
H(2B)	−0.0198	−0.2089	0.3431
Positional Parameters for Group Atoms			
N(21)	0.0000	0.0000	0.6281
C(22)	0.0685	0.0000	0.5640
C(23)	−0.0685	0.0000	0.5640
C(24)	0.0000	0.0000	0.3719
C(25)	0.0685	0.0000	0.4360
C(26)	−0.0685	0.0000	0.4360
H(22)	0.1178	0.0000	0.6101
H(23)	−0.1178	0.0000	0.6101
H(24)	0.0000	0.0000	0.2798
H(25)	0.1178	0.0000	0.3899
H(26)	−0.1178	0.0000	0.3899

[a] In the crystallographic refinement, the nitrogen atom of the pyridine solvate molecule was assumed to lie on the threefold axis. Subsequent NMR measurements indicate that it resides in the off-axis sites.

Table III. Bond Distances and Angles for $[Fe_3O(O_2CCH_3)_6(py)_3](py)$ at 200 K

Interatomic Distances

from	to	distance (Å)	from	to	distance (Å)
Fe	O	1.909 (2)	O(2)	C(2)	2.347 (14)
Fe	O(1)	2.064 (8)	C(1)	C(2)	1.518 (17)
Fe	O(2)	2.078 (7)	N(10)	C(12)	1.349 (12)
Fe	N(10)	2.215 (13)	N(10)	C(11)	2.384 (17)
O(1)	C(1)	1.232 (12)	C(11)	C(12)	1.360 (17)
O(1)	O(2)	2.229 (11)	C(11)	C(13)	1.381 (15)
O(1)	C(2)	2.338 (15)	C(12)	C(13)	2.347 (21)
O(2)	C(1)	1.247 (12)			

Bond Angles

from	thru	to	angles (deg)
O	Fe	O(1)	96.40 (21)
O(1)	Fe	N(10)	83.60 (21)
C(1)	O(1)	Fe	129.91 (75)
O(1)	C(1)	O(2)	128.09 (109)
O(1)	C(1)	C(2)	116.10 (107)
O(2)	C(1)	C(2)	115.82 (105)
C(12)	N(10)	C(12)	117.41 (155)
C(12)	N(10)	Fe	121.29 (77)
C(12)	C(11)	C(13)	117.73 (145)
N(10)	C(12)	C(11)	123.24 (135)
C(11)	C(13)	C(11)	120.55 (188)

(C–H = 1.00 Å). All hydrogen atoms were assigned isotropic temperature factors greater than or equal to that of the carbon atoms to which they are attached. The refinement converged at $R = 0.082$ and $R_w = 0.097$. The largest features in the final difference map were peaks of 0.61 e/Å^3 located near the iron atom. Positional parameters are given in Table II. Selected bond distances and angles are given in Table III.

Results and Discussion

Single-Crystal X-ray Structure of $[Fe_3O(O_2CCH_3)_6(py)_3](py)$ at 200 K. A drawing of the molecular structure is shown in Figure 1. The triply bridging oxygen atom is located on a site of 32 symmetry. The iron atom and the three coordinated pyridine ligands are located along the three crystallographic twofold axes. The three pyridine ligands are approximately coplanar with the Fe_3O plane.

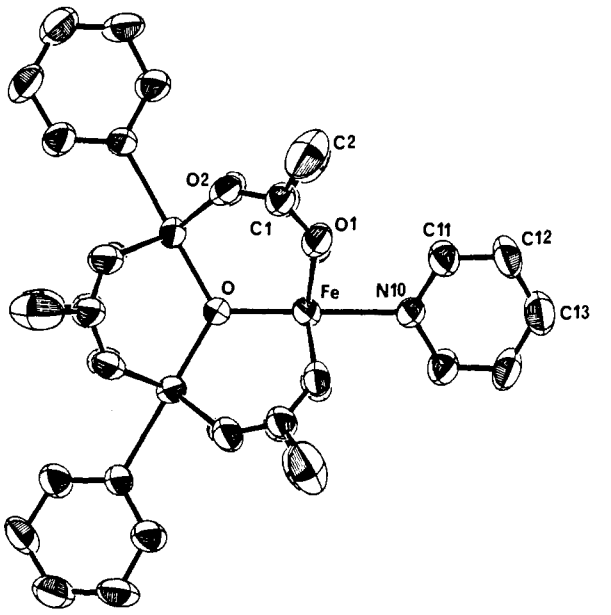

Figure 1. ORTEP plot of the molecular structure of $[Fe_3O(O_2CCH_3)_6(py)_3](py)$. Atoms are shown as 50% equiprobability ellipsoids.

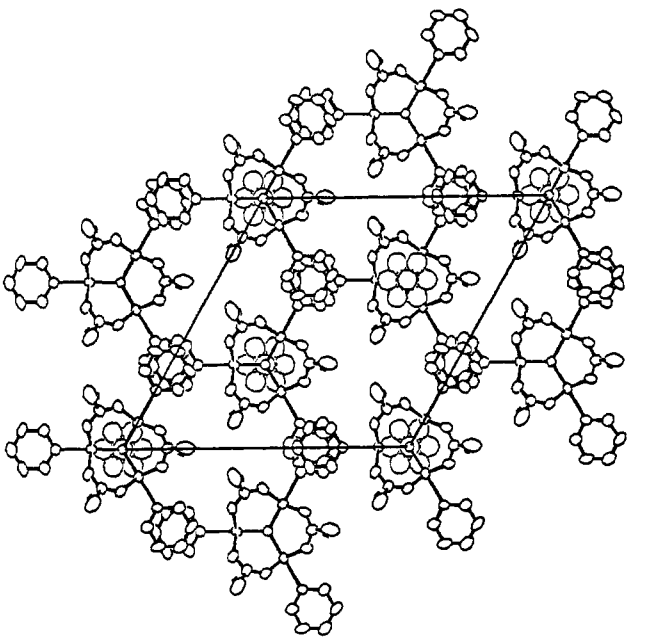

Figure 2. Packing arrangement in $[Fe_3O(O_2CCH_3)_6(py)_3](py)$. The crystallographic *c* axis is toward the viewer.

Table IV provides a comparison of the selected bond distances in this complex with those observed in closely related Fe_3O acetate complexes. The first two complexes listed in Table IV are mixed-valence complexes, and the other two contain three ferric ions. In $[Fe_3O(O_2CCH_3)_6(py)_3](py)$ the Fe–O(central) distance is found to be 1.909 (2) Å. This value is intermediate between the Fe^{II}–O [1.937 (6) Å] and Fe^{III}–O (1.889 Å) values observed[6a] in the valence-localized complex $[Fe_3O(O_2CCH_3)_6(3\text{-Me-py})_3](CH_3CN)$. The Fe–O(acetate) and Fe–ligand distances in the present complex can also be seen to be larger than those for the two $Fe^{III}{}_3O$ complexes. It is clear that the oxidation state of the iron ions in $[Fe_3O(O_2CCH_3)_6(py)_3](py)$ is intermediate between Fe^{II} and Fe^{III} at 200 K. This will be seen to be consistent with the 200 K Mössbauer spectrum.

As viewed down the *c* axis, the crystal-packing arrangement for $[Fe_3O(O_2CCH_3)_6(py)_3]$ is shown in Figure 2. Along the *c*

Table IV. Bond Distances (Å) for Some Fe_3O Acetate Complexes[a]

compound		Fe–O(central)	Fe–O(acetate)	Fe–L	ref
$[Fe_3O(O_2CCH_3)_6(py)_3](py)$		1.909 (2)	2.064 (8) 2.078 (7) ⟨2.071⟩	2.215 (13)	this work
$[Fe_3O(O_2CCH_3)_6(3\text{-Me-py})_3](CH_3CN)$	Fe^{II} Fe^{III}	1.937 (6) ⟨1.889⟩ (6)	2.071 (8) ⟨2.053⟩ (8)	2.225 (9) 2.234 (9)	*b*
$[Fe_3O(O_2CCH_3)_6(H_2O)_3]ClO_4$			⟨2.02⟩	⟨2.08⟩	*c*
$[Fe_3O(O_2CCMe_3)_6(MeOH)_3]Cl$		1.905 (5)	⟨2.04⟩ (2)	2.08 (1)	*d*

[a] Values in triangular brackets are averages of chemically equivalent distances. The numbers in the parentheses next to the average distances are based on the observed standard deviations. [b] See ref 6a. [c] Anzenhofer, K.; deBoer, J. J. *Recl. Trav. Chim. Pays-Bas* **1969**, *88*, 286. [d] Blake, A. B.; Frazer, L. R. *J. Chem. Soc., Dalton Trans.* **1975**, 193.

Table V. Mössbauer Fitting Parameters for $[Fe_3O(O_2CCH_3)_6(py)_3](py)$[a]

	δ,[b] mm/s			ΔE_Q, mm/s			% area			Γ,[c] mm/s		
T, K	Fe^{III}	Fe^{av}	Fe^{II}	Fe^{III}	Fe^{av}	Fe^{II}	Fe^{III}	Fe^{av}	Fe^{II}	Fe^{III}	Fe^{av}	Fe^{II}
11 (1)	0.521 (1)		1.260 (2)	1.012 (2)		2.101 (2)	65.2 (1)		34.8 (1)	0.124 (1)		0.124 (1)
51 (3)	0.529 (1)		1.221 (2)	1.013 (2)		1.902 (3)	64.4 (2)		35.6 (2)	0.147 (1)		0.151 (1)
105 (1)	0.542 (1)		1.221 (2)	0.989 (1)		1.726 (3)	67.2 (1)		32.8 (1)	0.158 (1)		0.165 (2)
106 (0.5)	0.541 (1)		1.220 (2)	0.994 (2)		1.731 (3)	65.4 (1)		34.6 (1)	0.155 (1)		0.176 (3)
109 (0.5)	0.544 (1)		1.218 (2)	0.994 (2)		1.690 (3)	66.8 (1)		33.2 (2)	0.164 (1)		0.187 (4)
111 (0.5)	0.544 (1)		1.225 (2)	0.993 (2)		1.672 (3)	67.2 (1)		32.6 (2)	0.164 (1)		0.191 (4)
112 (0.5)	0.542 (1)	0.901 (2)	1.224 (2)	0.968 (2)	0.274 (5)	1.876 (3)	50.2 (2)	30.4 (2)	19.4 (2)	0.152 (2)	0.162 (2)	0.160 (4)
113 (0.5)	0.545 (1)	0.893 (2)	1.224 (2)	0.962 (2)	0.221 (4)	1.821 (3)	48.6 (2)	33.0 (2)	18.4 (2)	0.148 (2)	0.164 (2)	0.150 (3)
115 (0.5)	0.545 (1)	0.882 (2)	1.224 (2)	0.961 (2)	0.209 (4)	1.778 (3)	48.0 (2)	34.0 (2)	18.0 (2)	0.148 (2)	0.160 (2)	0.152 (3)
117 (0.5)	0.547 (1)	0.870 (3)	1.13 (2)	0.960 (2)	0.231 (5)	1.701 (3)	47.0 (2)	32.0 (2)	21.0 (2)	0.142 (1)	0.156 (2)	1.154 (2)
138 (1)	0.552 (1)	0.861 (3)	1.201 (2)	0.941 (3)	0.230 (6)	1.651 (3)	52.0 (2)	29.0 (2)	19.0 (2)	0.134 (1)	0.158 (2)	0.147 (2)
158 (1)	0.589 (1)	0.845 (2)	1.130 (2)	0.867 (2)	0.214 (4)	1.216 (3)	52.8 (2)	30.0 (2)	17.2 (2)	0.135 (1)	0.156 (2)	0.147 (2)
168 (1)	0.599 (1)	0.813 (3)	1.046 (10)	0.805 (3)	0.217 (5)	0.976 (14)	46.0 (2)	41.2 (2)	12.8 (2)	0.132 (1)	0.184 (2)	0.147 (2)
										0.132 (1)	0.188 (3)	0.132 (2)
191 (1)		0.743 (1)			0.520 (1)			100			0.189 (4)	
											0.181 (4)	
297 (1)		0.772 (1)			0.761 (2)			100			0.175 (4)	
											0.174 (4)	
320 (1)		0.753 (1)			0.760 (2)			100			0.169 (3)	
											0.164 (3)	

[a] Peaks were least-squares fit to Lorentzian line shapes with equal areas for both components of a doublet; error in the last significant figure is given in parentheses. [b] Center shifts relative to Fe metal. [c] Half-width at half-maximum listed in order of increasing velocity of the peak.

axis, Fe_3O complexes and solvate molecules occupy alternating sites of 32 symmetry. That is, each pyridine solvate molecule is sandwiched between two Fe_3O complexes. The plane of the pyridine solvate molecule is perpendicular to the Fe_3O plane. As required by the presence of the C_3 axes along which the Fe_3O complexes are stacked, the pyridine solvate molecules are disordered. A view of one disordered solvate molecule sandwiched between two Fe_3O complexes is shown in Figure 3. Difference Fourier maps suggest that two of the atoms of the pyridine solvate lie on the C_3 axis. Alternate models of the disorder cannot, however, be excluded on the basis of crystallographic evidence. The large thermal parameters obtained for the atoms of the solvate molecule are consistent with a dynamic disorder.

In addition to the Fe_3O–solvate contacts, another significant intermolecular interaction exists between the pyridine ligands in adjacent stacks (see Figure 2). The separation between the centers of two nearly coplanar pyridine ligands on neighboring Fe_3O complexes is $c/3$, which at 200 K is 3.6 Å. Obviously there are appreciable intermolecular interactions. The present complex is isostructural with the previously reported $[Fe_3O(O_2CCH_3)_6(4\text{-Me-py})_3](\text{benzene})$.[8] The presence of the pyridine methyl substituent on the latter complex leads to a reduction in the ligand–ligand overlap.

^{57}Fe Mössbauer Spectroscopy. Variable-temperature Mössbauer spectra of $[Fe_3O(O_2CCH_3)_6(py)_3](py)$ are illustrated in Figure 4. At temperatures below ~105 K, two quadrupole-split doublets are seen, one is characteristic of high-spin Fe^{II} and the other of high-spin Fe^{III}. Parameters resulting from least-squares fit of the spectra to Lorentzian lines are listed in Table V. At 11 K the fitting parameters indicate that the Fe^{III} doublet is 65.2 (1)% of the spectral area, while the Fe^{II} doublet corresponds to 34.8 (1)%. This is very close to the expected 2:1 ratio of Fe^{III}:Fe^{II}. It is clear that this mixed-valence complex is localized on the Mössbauer time scale (~10^7–10^8 s^{-1}) below ~105 K. As the solid is heated

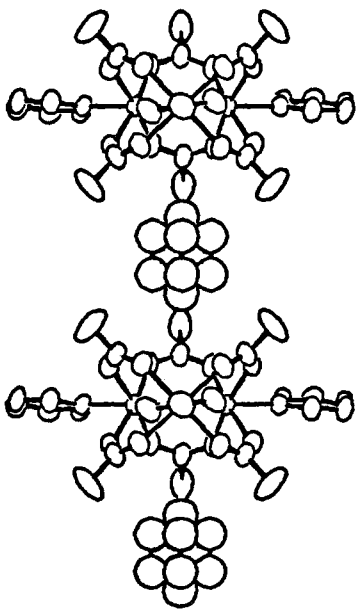

Figure 3. An ORTEP view of the stacking along the *c* axis. Each pyridine solvate molecule is aligned along the stacking direction *c* axis) with its ring plane parallel to the *c* axis and disordered in three positions.

the rate of intramolecular electron transfer increases such that above ~190 K the rate exceeds the ~10^7–10^8 s^{-1} rate which the Mössbauer technique can sense. At 320 K only a single doublet is seen with an isomer shift value that corresponds to an average oxidation state.

Four phase transitions have been identified in the heat-capacity measurement on this complex.[7,10] There are two groups of phase

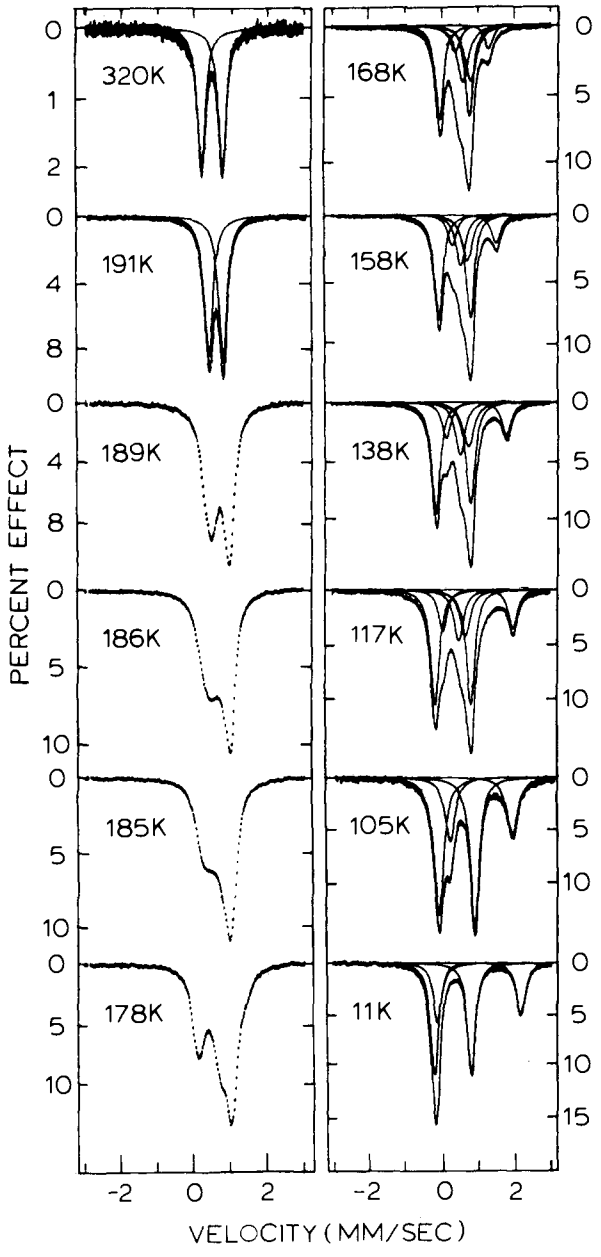

Figure 4. Variable-temperature ^{57}Fe Mössbauer spectra of $[Fe_3O(O_2CCH_3)_6(py)_3](py)$. Several spectra are least-squares fit to Lorentzian line shapes.

transitions present. The lower-temperature (LT) phase transitions (T_{C4} and T_{C3}) are first-order transitions at 111.4 and 112.0 K. Of the higher-temperature (HT) phase transitions with two C_p peaks, one is a higher-order transition at 191.3 K and the other is a first-order transition at 185.8 K. The higher-order phase transition actually starts at ~112 K and culminates at 191.3 K.

It is interesting that at the temperature of the LT-phase transitions (111–112 K) a third Mössbauer doublet characteristic of the average oxidation state appears suddenly (see Figure 5). The fitting parameters indicate that the doublet corresponding to the average oxidation state amounts to 30 to 40% of the spectral area between 112 and 168 K. The temperature of the HT-phase transitions (185–191 K) correspond to the temperature where the valences of the three iron ions become equivalent on the Mössbauer time scale. Moreover, the large temperature range (~112 to 191 K) over which the higher-order phase transition evolves corresponds exactly with the temperature region where the dramatic changes in the Mössbauer spectrum are occurring. That is, the transformation from a localized to a delocalized electronic structure occurs over a range of ~112 to ~190 K in the Mössbauer spectrum and this correlates well with the long C_p tail

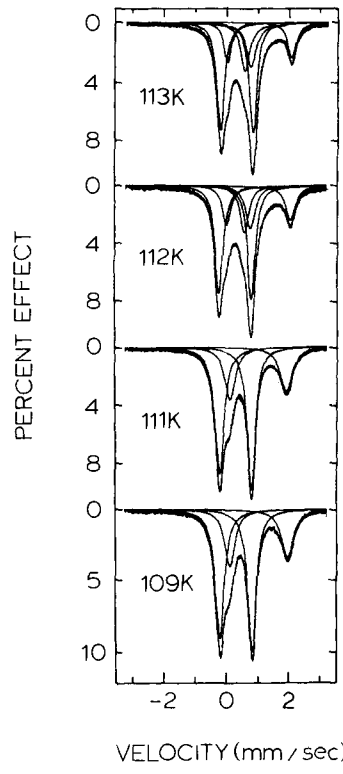

Figure 5. Variable-temperature ^{57}Fe Mössbauer spectra of $[Fe_3O(O_2CCH_3)_6(py)_3](py)$ in the vicinity of the low-temperature-phase transitions. The spectra are least-squares fit to Lorentzian line shapes.

spreading over ~115 to ~191 K in the heat-capacity data.

It has been suggested that the LT-phase transition is an order–disorder phase transition.[10,18] At temperatures below this phase transition point the triangular Fe_3O complexes each have a static distortion reflecting the iron valence states. One iron is Fe^{II} and the other two are Fe^{III}. These distorted complexes are ordered in domains, e.g., homogeneous regions of crystallite where the distortions of the Fe_3O triangular frameworks are ordered in some sense. At the LT-phase transition these domains disappear and the sense of distortion becomes randomly distributed throughout the crystallite. The packing arrangement of this complex involves stacks of pyridine ligands with an interplanar separation of $c/3 = 3.6$ Å at 200 K. The pyridine ligands from neighboring molecules experience appreciable π–π overlap (see Figure 2) and this could lead to cooperativity and the first-order phase transitions at 111.4 and 112.0 K. The microscopic origin for *two* phase transitions is not known. The third doublet that appears in the Mössbauer spectrum at ~112 K is attributable to Fe_3O complexes which are electronically delocalized. The first-order phase transitions at ~112 K could lead to a change in the ground-state potential-energy surface for a single Fe_3O complex such that above this temperature the zero-point energies of the *three* electronically localized distorted states (i.e., $Fe^{II}{}_AFe^{III}{}_BFe^{III}{}_C$, $Fe^{III}{}_AFe^{II}{}_BFe^{III}{}_C$, and $Fe^{III}{}_AFe^{III}{}_BFe^{II}{}_C$) and the *one* electronically delocalized nondistorted state become comparable in magnitude. This situation of having *four* minima of equal energies in the ground-state potential-energy diagram of a mixed-valence Fe_3O complex has been theoretically predicted recently.[18-21]

Of the two HT-phase transitions, one is a first-order phase transition at 185.8 K and the other is a higher-order phase transition which evolves over an extensive temperature range (~112 to 191 K). It is clear from the Mössbauer results that

(18) Kambara, T.; Hendrickson, D. N.; Sorai, M.; Oh, S. M. *J. Chem. Phys.* **1986**, *85*, 2895.
(19) Borschch, S. A.; Kotov, I. N.; Bersuker, I. B. *Chem. Phys. Lett.* **1982**, *89*, 381.
(20) Launay, J. P.; Babonneau, F. *Chem. Phys.* **1982**, *67*, 295.
(21) Cannon, R. D.; Montri, L.; Brown, D. B.; Marshall, K. M.; Elliott, C. M. *J. Am. Chem. Soc.* **1984**, *106*, 2591.

this higher-order phase transition involves an electronic localization–delocalization phase transition. Fe_3O complexes are thermally activated such that they can convert from one vibronic state to another by overcoming a potential-energy barrier. It is also likely that Fe_3O complexes are tunneling from one vibronic state to another. Because it is likely that there are appreciable intermolecular interactions, e.g., the solvate-molecule-propagated interaction of two nearest-neighbor Fe_3O complexes in a stack, there would be a cooperativity in the transformation from electronically localized to electronically delocalized Fe_3O complexes.

The first-order phase transition at 185.8 K has been suggested[10,18] to involve the onset of motion in the pyridine solvate molecules. Rapid rotation of these solvate molecules about the C_3 axis is required in order to have a C_3 site symmetry for the Fe_3O complexes. In the absence of this high symmetry the ground-state potential-energy surface for each Fe_3O complex could have appreciable zero-point energy differences between three electronically localized vibronic states. Such zero-point energy differences could obviously increase the barrier(s) for intramolecular electron transfer or they could reduce the rate of tunneling and the Fe_3O complex would likely be localized in one state, $Fe^{II}_AFe^{III}_BFe^{III}_C$, for example. Definitive evidence for the motion of the pyridine solvate molecules is presented in the next section.

^{2}H NMR Spectroscopy. Experiments were carried out on two different deuterated forms of the complex: $[Fe_3O(O_2CCD_3)_6(py)_3](py)$ and $[Fe_3O(O_2CCH_3)_6(C_5D_5N)_3](C_5D_5N)$. The deuterated acetate groups in the first form serve as good probes of the electronic structure of the mixed-valence Fe_3O complex in the solid state, whereas the deuterated pyridines in the second form can be used to gauge solvate or ligand dynamics.

There are two types of interactions apparent in a ^{2}H NMR spectrum of a paramagnetic compound. The nuclear quadrupole interaction of the ^{2}H ($I = 1$) nucleus gives rise to a doublet for each different deuterium site. The mixed-valence Fe_3O complexes are paramagnetic with a $S = 1$ ground state as well as appreciable thermal population of excited states at room temperature.[22-24] There is a through-space dipolar interaction of the magnetic moment of the unpaired electrons of the Fe_3O complex with the nuclear magnetic moment of the ^{2}H nucleus. As a consequence, the quadrupole-split ^{2}H NMR doublet is shifted from zero frequency (defined as the ^{2}H NMR frequency in diamagnetic molecules) by this dipolar interaction. The dipolar interaction depends on the magnitude of the magnetic moment associated with the unpaired electrons and varies inversely with the cube of the distance between the nuclear and electron spin moments. It also depends on the angle between the principal components of these two moments. Additional general comments about the ^{2}H NMR of paramagnetic metal complexes are available in a previous paper.[8]

A single crystal of $[Fe_3O(O_2CCD_3)_6(py)_3](py)$ of the dimensions $1 \times 1 \times 1$ mm was oriented in a 5.9-T magnetic field. That is, a single crystal was allowed to turn in a 5.9-T magnetic field until it had its easy axis (i.e., principal component) of magnetic susceptibility aligned along the magnetic field. As is evident in Figure 2, all Fe_3O complexes have the same orientation in the crystal. They are stacked along C_3 axes. In this type of packing arrangement the principal components of the magnetic susceptibility tensor of each Fe_3O complex are aligned throughout the crystal. Since the crystal does turn in an external magnetic field, each Fe_3O complex must be magnetically anisotropic.

The direction of the principal component of the bulk (also for a single complex) magnetic susceptibility tensor can be identified by inspection of the ^{2}H NMR spectra shown in Figure 6. At temperatures above ~188 K the spectrum consists of a single quadrupole-split doublet. This clearly indicates that with the crystal oriented in the fashion described above all six CD_3 groups

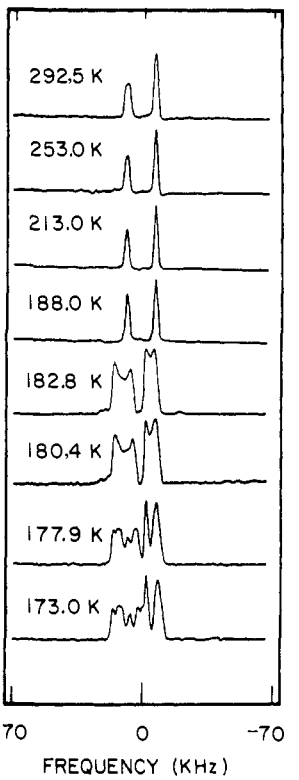

Figure 6. Variable-temperature single-crystal ^{2}H NMR spectra for $[Fe_3O(O_2CCD_3)_6(py)_3](py)$. Only the methyl groups on the acetate bridges are deuterated. The single crystal, ~1 mm on an edge, is oriented in the magnetic field such that H_0 is along the principal component of the magnetic susceptibility tensor.

of a Fe_3O complex are equivalent in terms of dipolar and quadrupolar coupling interactions. This is only possible when the crystal is oriented with its crystallographic c axis (stacking direction) along the magnetic field. In this orientation, the angle between the magnetic field and the direction of the principal component of the quadrupole coupling tensor is identical for all six CD_3 groups of a D_{3h} symmetry Fe_3O complex. Furthermore, when the Fe_3O complex is electronically delocalized all six CD_3 groups will experience equivalent dipolar interactions.

In the solid state the CD_3 groups of a Fe_3O complex are rotating rapidly about their local C_3 axes at temperatures even as low as 100 K. For such a rapidly rotating CD_3 group, the (motionally averaged) residual quadrupole splitting tensor would have components of $\langle V_{zz} \rangle = 42$ kHz, $\langle V_{xx} \rangle = -21$ kHz, and $\langle V_{yy} \rangle = -21$ kHz assuming that the quadrupole coupling constant for a static CD_3 group is 165 kHz.[25] Thus, when the magnetic field is directed perpendicular to the local C_3 axis of the rapidly rotating CD_3 group, the observed quadrupole splitting is expected to be 21 kHz. As can be seen in Figure 6, in the temperature range of 188.0–292.5 K the residual quadrupole coupling is observed to be 11.3 kHz $[=1/2(\nu_1 - \nu_2)]$. From this experimental value the angle between the magnetic field and the principal component of the residual quadrupole tensor is calculated to be ~45°. From the 200 K X-ray structure of $[Fe_3O(O_2CCH_3)_6(py)_3](py)$ the angle between the local C_3 axis of the CD_3 group and the crystallographic c axis is found to be ~45°. It is clear that this crystal aligns with it's c axis along the magnetic field.

When the deuterated acetate crystal which is oriented along the easy axis is cooled, the spectrum consisting of a single doublet above 188.0 K changes eventually to become a spectrum with at least four and likely six quadrupole-split doublets below ~178 K. In the temperature range of 180–183 K spectral features are broad, indicating exchange broadening. As will be seen below,

(22) Jones, D. H.; Sams, J. R.; Thompson, R. C. *J. Chem. Phys.* **1984**, *81*, 440.
(23) Tsukerblat, B. S.; Belinskii, M. I.; Kuyavskaya, B. Ya. *Inorg. Chem.* **1983**, *22*, 995.
(24) Wrobleski, J. T.; Dziobkowski, C. T.; Brown, D. B. *Inorg. Chem.* **1981**, *20*, 671.
(25) (a) Seelig, J. *Q. Rev. Biophys.* **1977**, *10*, 353. (b) Barnes, R. G. *Advances in Nuclear Quadrupole Resonance*; Smith, J. A. S., Ed.; Heyden: London, 1972; Vol. 1.

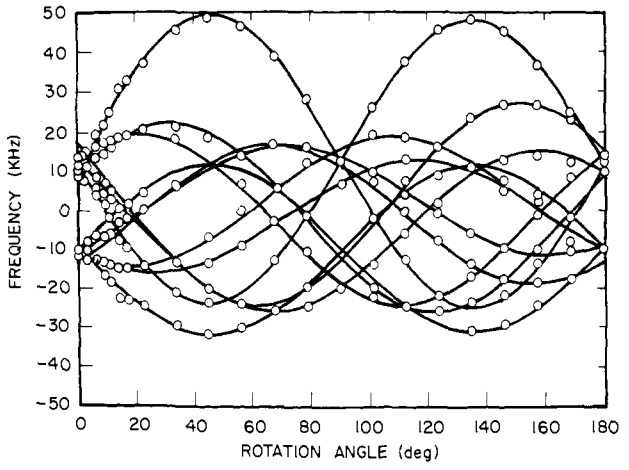

Figure 7. Results of a 293 K single-crystal (~1 mm on an edge) ^2H NMR study of $[Fe_3O(O_2CCD_3)_6(py)_3](py)$. The axis about which the rotation was carried out is perpendicular to the crystallographic *c* axis. The circles indicate the NMR peak positions, whereas the solid lines resulted from least-squares fitting to the angular dependencies expected for six doublets.

in this temperature range the pyridine solvate molecules stop rotating about the crystallographic *c* axis (C_3 stacking axis). The ground-state potential-energy surface of each Fe_3O complex changes from being symmetric above ~188 K (three equal-energy distorted states) to being asymmetric below this temperature (one energetically preferred distortion where one iron is Fe^{II}). The rate of intramolecular electron transfer is less than the ^2H NMR time scale at ~173 K, for it can be seen that, excluding the overlapping of components of doublets, the line widths are comparable to those seen in spectra taken at temperatures of ~188 K or higher. From the Uncertainty Principle or exchange theory in the slow limit the product of the uncertainty in frequency or line width ($\Delta\nu$) and the lifetime (τ) is of the order of $1/2\pi$, i.e., $\tau\Delta\nu \approx 1/2\pi$. With an approximate value for the line width of $\Delta\nu = 5$ kHz, a value of $\tau = 3.2 \times 10^{-5}$ s can be calculated. This means that the rate of intramolecular electron transfer or any averaging process is less than $\sim 3.1 \times 10^4$ s^{-1} at ~173 K. Thus, from the combination of Mössbauer and NMR data we infer that the rate of intramolecular electron transfer exceeds $\sim 10^7$ s^{-1} at ~190 K but falls off to less than $\sim 3.1 \times 10^4$ s^{-1} at ~173 K.

Knowledge of the detailed origin of the additional spectral splitting in the 173.0 K spectrum (see Figure 6) of the deuterated-acetate single crystal awaits further low-temperature studies. When the Fe_3O complexes change from electronically delocalized equilateral triangular complexes to electronically localized isosceles (distorted) triangular complexes, it is possible that the orientations of the six CD_3 groups of a Fe_3O complex will change relative to the crystallographic *c* axis (magnetic field direction). Even a small change in the angle is important in this angular range. With an electronically localized Fe_3O complex there would be two types of deuteron sites relative to the quadrupole interaction, one where a CD_3 group is between two Fe^{III} ions and another where a CD_3 group is part of an acetate anion bridging between an Fe^{III} and an Fe^{II} ion. The site symmetry of a localized Fe_3O complex would lead to two different quadrupole-split doublets in a ratio of 2:1; however, examination of Figure 6 shows there are many doublets present in the 173.0 K spectrum. The dipolar interaction will lead to many more than two different types of deuteron sites. It is important to note that the deuterons of a given CD_3 group are also almost as close to *two* iron ions of two neighboring Fe_3O complexes as they are to two iron ions in their own complex. Dipolar interactions are present in the solid state between a given deuteron and the unpaired electron density associated with *three* Fe_3O complexes. As a result of these through-space dipolar interactions there will be several different deuteron sites in the solid.

The results of a room temperature (293 K) single axis rotation study of the deuterated acetate single crystal are shown in Figure 7. The sample was magnetically oriented in paraffin and subsequently rotated about an axis perpendicular to H_0. Rotation patterns for 12 lines resulting from the 6 methyl groups are resolved. To determine the quadrupole and paramagnetic couplings, the 12 lines must be paired to give 6 doublets. This pairing was substantially simplified by using the magnetically oriented crystal, which at $\theta = 0°$ has a single doublet. As θ is increased, each line of the doublet breaks into as many as 6 lines, each of which is then paired with a line originating from the other 0° line. Furthermore, since the spectral shifts are dominated by quadrupolar splitting, a line displaying a certain frequency must be paired with a line with shift of similar magnitude but opposite sign for all values of θ in which the shift is more than a few kHz. The full paramagnetic and quadrupolar tensors were then determined from this single axis rotation data by utilizing the threefold symmetry of the molecule. The residual principal components for the axial quadrupolar coupling are -20 ± 1.5 and 40 ± 1.5 kHz, in excellent agreement with the values expected for methyl groups reorienting about their C_3 axis and otherwise static. Direct inspection of the rotation plot, Figure 7, shows that the sample was oriented, perhaps fortuitously, such that two of the methyl rotation axes lie in the goniometer rotation plane and thus at some θ have their methyl axes along H_0 with quadrupolar splittings of ±41 kHz. This occurs at $\theta = 45°$ and 135°, confirming the methyl orientation calculated from the 0° quadrupolar splitting as well as from the X-ray structure. Spectra obtained at 173 K are of very similar overall spectral width, and thus methyl rotation persists in the low-temperature phase at this temperature.

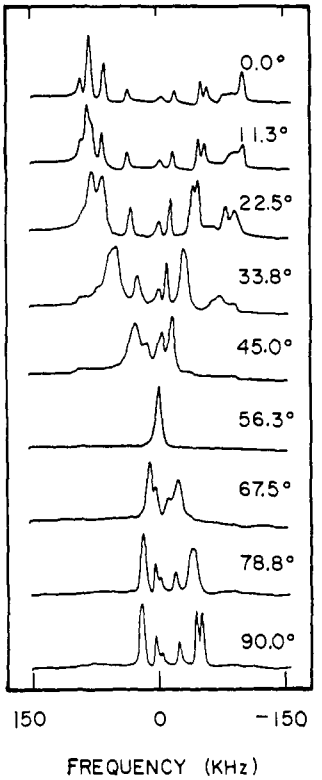

Figure 8. ^2H NMR spectra of the magnetically oriented microcrystalline sample of $[Fe_3O(O_2CCH_3)_6(C_5D_5N)_3](C_5D_5N)$ at 273 K. The angles represent those between the magnetic field and the "frozen" easy axis (crystallographic *c* axis). The microcrystalline sample was oriented in the magnetic field in a hexadecane matrix.

The paramagnetic tensor, with principal values of -6.9 ± 1.5, -2.5 ± 1.5, and 8.8 ± 1.5 kHz, is decidely non-axial. As discussed previously,[8] the non-axiality of this dipolar coupling is expected since the cluster **g** tensor is not isotropic (the samples orient in the magnetic field) and the magnetic dipole–dipole vectors are not coaxial with the easy axis.

The deuterated pyridine sample was examined to monitor directly the motion of pyridine solvate molecules. Figure 8 shows a series of results obtained by suspending a microcrystalline sample

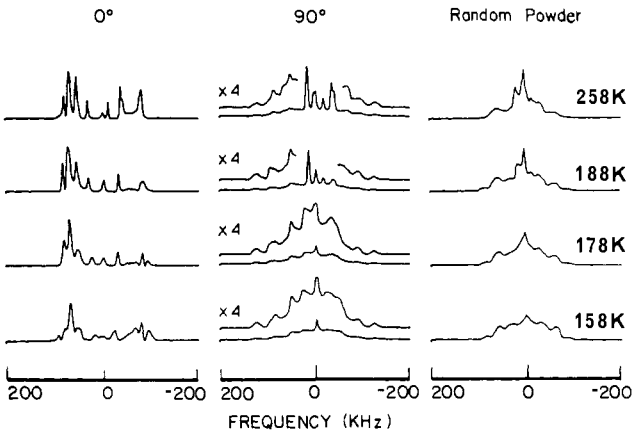

Figure 9. Variable-temperature ^2H NMR spectra of $[Fe_3O(O_2CCH_3)_6(C_5D_5N)_3](C_5D_5N)$ near the HT-phase transitions (185–191 K): magnetically oriented microcrystalline sample with $\theta = 0°$ where the "frozen" easy axis is parallel to H_0; magnetically oriented microcrystalline sample with $\theta = 90°$ where the "frozen" easy axis is perpendicular to H_0; random powder spectra.

of $[Fe_3O(O_2CCH_3)_6(C_5D_5N)_3](C_5D_5N)$ in hexadecane (mp = 291 K), orienting the sample in the NMR magnet at $T > 291$ K and then obtaining a series of spectra at 273 K by rotating the "frozen" easy axis about the magnetic field through various angles. Even though such magnetically oriented samples are typically disordered in the plane perpendicular to the easy axis, sharp lines are observed for the 0° orientation. This occurs because the resonance frequencies are determined by the zz component of the lab-frame quadrupolar and paramagnetic tensors which, when the easy axis is along H_0, are invariant to the arbitrary orientation about H_0 effected by the disorder. For the 0° spectrum, we distinguish three doublets or groups of doublets. The outermost group have quadrupole splittings near 70 kHz, as expected[26] for stationary aromatic deuterons with their C–D vectors perpendicular to H_0 and can thus be assigned to the three coordinated pyridine groups since from the X-ray structure the pyridine planes are known to be essentially normal to the C_3 and easy axes (see Figures 2 and 3). The inner doublets show smaller quadrupolar couplings of 52 and 22 kHz, equivalent paramagnetic shifts of 10 kHz, and an intensity ratio (to the nearest integer) of 4:1. Furthermore, the upfield component of the doublet with the 52-kHz coupling is split for orientations near 0°. Integrated intensities show that the ratio of the outer doublet to the sum for the two inner doublets is 2:1 rather than the expected 3:1 if the inner doublets are assigned to the solvate pyridine deuterons. This results from the rather poor excitation bandwidth of the 4-pulse echo experiment used to obtain these rather wide spectra. For the less demanding 2-pulse solid echo, with the 90° pulse widths of 2.7 μs used here, the doublets at 70 kHz will be attenuated by a factor of 0.8 relative to the inner doublets at 22 kHz.[27] Thus, the signal intensities and the quadrupolar frequencies are consistent with the above resonance assignments.

As the goniometer angle is increased from 0°, the outer doublet broadens as expected since the (macroscopic) disorder of the coordinated pyridines is increasingly projected onto H_0. At an angle of 90° the plane of disorder is perpendicular to H_0, all orientations are possible, and the vertically expanded spectra in Figure 9 show the broad spectral features extending over the full range of ±140 kHz expected for deuterons on a static aromatic group. The inner doublets, however, remain sharp for all orientations. This occurs only if their respective quadrupolar and paramagnetic tensors are axially symmetric about the easy axis which, as discussed above, is along the crystallographic C_3 axis. Such a constraint on orientation makes these tensors invariant to the disorder inherent to the magnetically ordered sample.

(26) (a) Rice, D. M.; Wittebort, R. J.; Griffin, R. G.; Meirovitch, E.; Stimson, E. R.; Meiwald, Y. C.; Freed, J. H.; Scheraga, H. A. *J. Am. Chem. Soc.* **1981**, *103*, 7707. (b) Meirovitch, E.; Belsky, I.; Vega, S. *J. Phys. Chem.* **1984**, *88*, 1522.

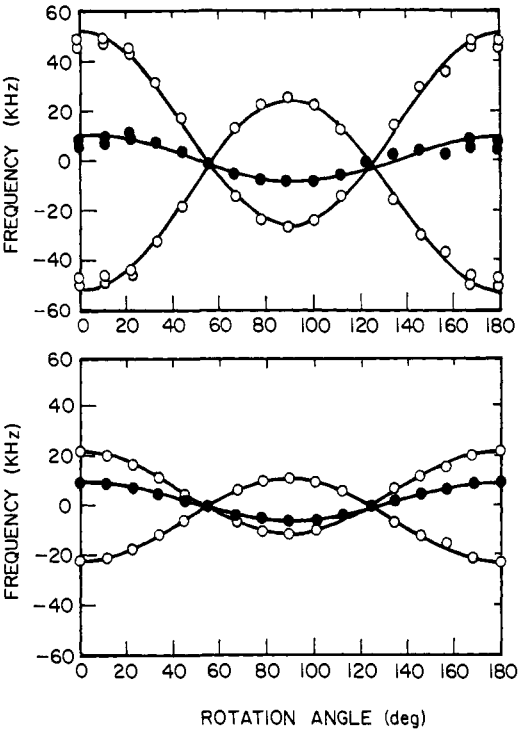

Figure 10. Rotation patterns of the quadrupole splitting (○) and paramagnetic shifts (●) of the solvate pyridine deuterons in $[Fe_3O(O_2CCH_3)_6(C_5D_5N)_3](C_5D_5N)$ at 273 K. The rotation axis is perpendicular to H_0. The top trace is for the doublet having the larger quadrupole splitting and the bottom trace is for the doublet having the smaller quadrupole splitting.

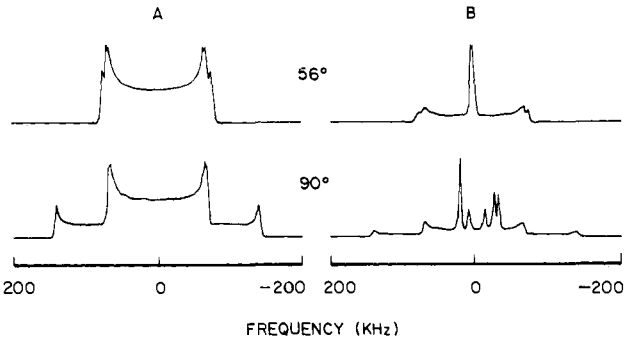

Figure 11. Simulations of the coordinated pyridine (A) and combined coordinated and solvate pyridine (B) spectra for magnetically oriented samples of $[Fe_3O(O_2CCH_3)_6(C_5D_5N)_3](C_5D_5N)$ at goniometer angles of 56° and 90°. The simulations in part B are to be compared with the 56.3° and 90° spectra of Figure 8.

Shown in Figure 10 are rotation plots for the quadrupolar, $\nu_Q = 1/2(\nu_1 - \nu_2)$, and paramagntic, $\nu_P = 1/2(\nu_1 + \nu_2)$, frequencies confirming the expected rotation behavior for the two inner doublets, namely the plots are symmetric about 90° and the splittings vanish at the magic angle and its complement. Integrated intensities for the sharp doublets are, within 25%, constant as the angle is varied. This fortuitous orientation of the residual quadrupolar coupling and paramagnetic tensors for the solvate deuterons has been observed[8] in the related compound $[Fe_3O(O_2CCH_3)_6(4\text{-Me-py})_3](C_6D_6)$ and results from the symmetry of dynamic averaging about the crystallographic C_3 axis.

We conclude that the five solvate deuterons show essentially two residual quadrupolar tensors coaxial about the crystallographic C_3 axis with unique components of $\langle V_{zz}\rangle = 22$ kHz ($\langle V_{xx}\rangle = \langle V_{yy}\rangle = -11$ kHz) and $\langle V_{zz}\rangle = 52$ kHz ($\langle V_{xx}\rangle = \langle V_{yy}\rangle = -26$ kHz). Furthermore, one deuteron gives rise to the 22-kHz coupling, whereas four deuterons contribute to the 52-kHz coupling.

To further confirm this description of these spectra, simulations are shown in Figure 11 for the 56° and 90° orientations. For

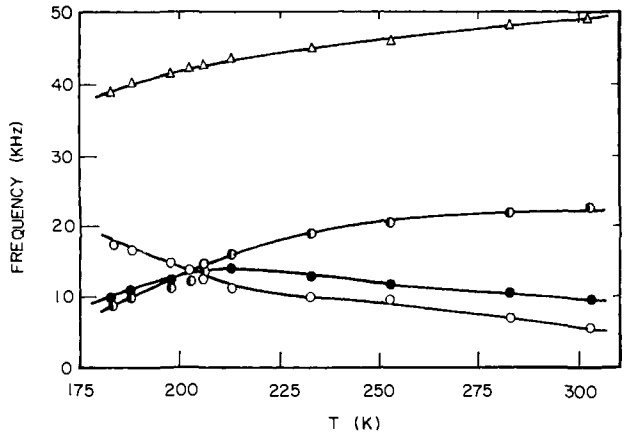

Figure 12. Plots of the quadrupolar, ν_Q, and paramagnetic, ν_P, couplings vs. temperature for the two doublets from the pyridine solvate: △ and ◐ are ν_Q and ○ and ● are ν_p for the ortho or meta and para deuterons, respectively.

simplicity, we assume that the C–D vectors of the coordinated pyridines are randomly distributed in the plane perpendicular to the easy axis and neglect the much smaller paramagnetic shifts in calculating the patterns arising from these deuterons. The resonance frequencies are given by

$$\nu = \pm 1/2\nu_Q[\sin^2\theta(3\cos^2\phi - 1) + \cos^2\theta] \qquad (1)$$

where θ is the goniometer angle and ν_Q is the quadrupole coupling constant (taken as 140 kHz for aromatic deuterons). The patterns in Figure 11A are obtained by numerically integrating (summing) Gaussian lines at center frequencies given by eq 1 as a function of the azimuthal angle ϕ, which is assumed to be equiprobable over the range of 0–360°. In Figure 11B single Gaussian lines at the frequencies observed in the corresponding experimental spectra of Figure 8 are added to the simulation in Figure 11A. The relative intensities based on the above assignments are used and the spectra are corrected for the excitation efficiency of the two-pulse solid echo.[27] Within these approximations the simulations confirm the particular conclusion that at the 90° goniometer orientation, the intense, sharp spectral features arise only from the solvate pyridine deuterons. In Figure 12 are shown the plots of ν_Q and ν_P vs. temperature for the two doublets from the pyridine solvate molecule.

In the related compound $[Fe_3O(O_2CCH_3)_6(4\text{-Me-py})_3](C_6D_6)$ all six solvate deuterons were observed[8] to be equivalent with a quadrupolar coupling of 34 kHz, intermediate between the two couplings observed here for the pyridine solvate. This observation was quantitatively interpreted to result from axial reorientation about both the local benzene C_6 axis (making all deuterons equivalent) and the crystallographic C_3 axis (to give the proper tensor orientation and magnitude). In the present case, the symmetric reorientation about the C_3 axis remains as discussed above but, since two distinct quadrupolar couplings are observed, reorientation about the ring normal is not unrestricted. These results are understood as follows: To account for the doublet intensities we assume that the less intense doublet with the 22-kHz splitting (0° orientation) results from the single deuteron para to the nitrogen atom of the pyridine solvate and the fourfold more intense doublet with 52-kHz splitting is from the ortho and meta deuterons. On average, the angle between the C_3 axis and the C–D vectors must be smaller and nearly equivalent for the ortho or meta deuterons than for the para deuterons in order that the residual coupling is larger for the ortho and meta sites. Shown in Figure 13 are illustrations of two dynamical processes which are in qualitative agreement with these observations. Both models involve discrete jumps among six orientations. In Figure 13A,B the 3-fold jumps about the crystallographic C_3 axis are not shown. Both models predict the same unique principal components of 18

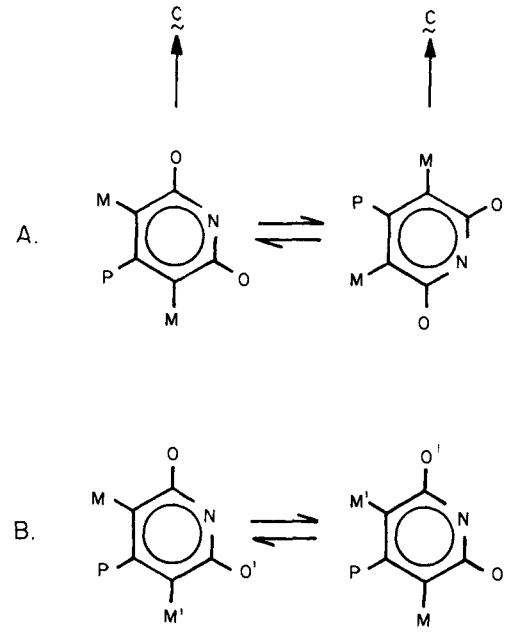

Figure 13. Two models for the solvate molecule dynamics in the HT phase of $[Fe_3O(O_2CCH_3)_6(py)_3](py)$. In both parts A and B the dynamics (threefold jumps) about the crystallographic c axis are not shown. In part A the pyridine solvate molecule makes an in-plane jump by 60°, whereas in part B the plane of the pyridine solvate molecule rotates by 180° about its para axis. The symbols O, M, and P (and primed versions) refer to deuterons in positions ortho, meta, and para to the nitrogen atom, respectively.

kHz for the para deuteron and 62 kHz for the four ortho and meta deuterons, in reasonable agreement with the experimental values. Futhermore, in accord with the X-ray results, both models have two atoms on the C_3 axis. In Figure 13A the ring makes at 60° in-plane jump and the para C–D bond is, on the average, perpendicular to the C_3 axis and equivalently oriented with respect to the two clusters between which it is packed. The jump illustrated in Figure 13B is a 180° ring flip about the solvate symmetry axis. Compared to that in Figure 13A, this jump would appear more sterically hindered.

Temperature-dependent spectra over the range from 258 to 158 K are shown in Figure 9 for a magnetically oriented sample at the goniometer angles of 0° and 90° and for a randomly oriented powder sample. For the 0° orientation the spectral lines are resolved at all temperatures above and below the phase transition which occurs in the range of 185–190 K. Some broadening occurs as the temperature is lowered. From the spectra run at the 0° orientation the quadrupolar splittings and paramagnetic shifts determined from the two doublets assigned to the solvate deuterons are plotted as a function of temperature in Figure 12. The paramagnetic shifts for the para and ortho or meta deuterons are nearly equivalent for $T > 200$ K and show some non-Curie law behavior at the phase transition. In contrast to the results for $[Fe_3O(O_2CCH_3)_6(4\text{-Me-py})_3](C_6D_6)$, the quadrupole splittings for the pyridine solvate in $[Fe_3O(O_2CCH_3)_6(py)_3](py)$ decrease as the temperature is lowered. They do not, however, change dramatically in the range of the phase transition. In contrast, the spectra obtained at the 90° orientation (Figure 9) show a singular change in the range of the HT-phase transition. The well-resolved solvate doublets observed above the HT-phase transitions are completely broadened into powder-like patterns indistinguishable from the patterns due the coordinated pyridines at temperatures below the HT-phase transitions. Since the condition for observing the resolved solvate doublets at the 90° orientation is the presence of rapid axially symmetric averaging about the C_3 axis, this observation is readily interpreted as a change from a state of dynamical disorder ($\tau_C^{-1} > 10^5\ s^{-1}$) of the solvate orientation about the C_3 axis for $T > T_C$ to a state in which the solvate has a static ($\tau_C^{-1} < 10^3\ s^{-1}$) orientation with respect to this C_3 axis for $T < T_C$. Since the breadth of the pattern due to

(27) Bloom, M.; Davis, J. H.; Valic, M. I. *Can. J. Phys.* **1980**, *58*, 1510.

solvate deuterons is not resolved in the low-temperature phase, whether the solvate is completely stationary on the ^2H NMR time scale cannot be determined here. As shown in Figure 12, when the sample is oriented with the c axis along H_0, solvate deuteron quadrupolar couplings do change (small continuous decrease) as the temperature is lowered through the phase transition temperature. Consequently, the change in dynamics at the transition cannot be described as only a loss of rapid axially symmetric averaging about this axis. From the vertical expansions of the spectra in Figure 9 ($\theta = 90°$) it is seen that the broad features of the spectra arising from the coordinated pyridines show little change from 258 to 158 K. Shown in Figure 9 are powder patterns which confirm the spectral change at T_C. Again, the broad features extending from ±60 to ±150 kHz are due to the ligands and show little change with T, whereas the narrower averaged patterns from the solvate are concentrated in the center of the spectrum and change substantially as the phase transition occurs.

It is of particular interest to compare the results previously reported[8] for $[Fe_3O(O_2CCH_3)_6(4\text{-Me-py})_3](C_6D_6)$ with those reported here for the isostructural complex containing a pyridine solvate. In the complex with a symmetric solvate (i.e., benzene), the solvate remains dynamically disordered at all temperatures down to 153 K and there is no dramatic change in the electronic properties of the nearby Fe_3O complex. Combined with results from Mössbauer spectroscopy and ^2H NMR of the deuterated acetate complex, these experiments show a straightforward connection between the onset of solvate dynamics and a dramatic change in the cluster electronic properties.

Conclusions and Comments

The factors affecting the rate of *intra*molecular electron transfer in $[Fe_3O(O_2CCH_3)_6(py)_3](py)$ in the solid state have been examined in detail. The 200 K X-ray structure shows that the Fe_3O complexes are stacked along a threefold crystallographic axis. The pyridine solvate molecules are intercalated into the stacks such that the plane of the pyridine solvate is perpendicular to the Fe_3O planes; the solvate molecules are disordered about the C_3 axis. A structural transformation that appears to be associated with loss of the crystallographic C_3 axis takes place below 200 K. Four phase transitions (111.4, 112.0, 185.8, and 191.3 K) have been detected[10] in the heat-capacity data for the compound; the first three are first-order phase transitions, whereas the highest temperature one is a higher order phase transition which starts at ~112 K and culminates at 191.3 K. These phase transitions can be grouped into two basic phase transitions: the LT-phase transition and the HT-phase transition.

There are good correlations between the temperatures of the LT-phase and HT-phase transition and occurrences in the variable-temperature Mössbauer data. As the sample temperature is increased the Mössbauer spectrum converts at the LT-phase transition temperature from two doublets (high-spin Fe^{II} and Fe^{III}) to three doublets, where the third doublet corresponds to that for a theoretically predicted form of the Fe_3O complex in which all iron ions are equivalent. The LT-phase transition is an order–disorder phase transition wherein intermolecular interactions are overcome by thermal energies and there is a conversion from a phase consisting of electronically localized complexes to give a disordered mixture of electronically localized and nondistorted (valence-equivalent) Fe_3O complexes in a crystallite.[18]

One component of the HT-phase transition involves an electronic localization–delocalization phase transition starting from ~112 and culminting at 191.3 K. Fe_3O complexes are thermally excited both to overcome barriers for electron transfer as well as to experience an increasing rate of electron and nuclear tunneling. ^2H NMR studies on a single crystal with deuterated acetate groups showed that the Fe_3O complexes are electronically delocalized above ~188 K, whereas the rate of intramolecular electron transfer decreases to less than $\sim 3.1 \times 10^4$ s^{-1} at ~173 K. The Mössbauer data show that the rate of electron transfer exceeds $\sim 10^7$ s^{-1} at ~190 K.

Finally, ^2H NMR studies of magnetically oriented microcrystalline $[Fe_3O(O_2CCH_3)_6(C_5D_5N)_3](C_5D_5N)$, where the pyridines are deuterated, have definitively demonstrated that the pyridine solvate molecules experience an abrupt onset of rotation about the crystallographic threefold axis at the temperature of the first-order component of the HT-phase transition. This onset of rapid rotation of the solvate molecule about the C_3 axis very likely changes the ground-state potential-energy surface for each Fe_3O complex. The conversion to an environment with threefold symmetry would lead to the case that the ground-state potential-energy surface has a threefold symmetry as well. The three states where the "extra" electron is itinerating at one of the three iron ions would have the same zero-point energies. This relatively sudden change in the ground-state potential-energy surface has a dramatic impact on the rate of intramolecular electron transfer. When the three zero-point energies are not equal below the HT-phase transition, the electron transfer is slow. Symmetrizing the ground-state potential-energy surface could lead to a dramatic increase in the rate of quantum-mechanical tunneling.

Acknowledgment. We are grateful for support from National Institutes of Health Grants HL13652 (D.N.H.) and GM35329-01 (C.E.S.) and from National Science Foundation Grants PCM-8118912 (R.J.W.) and CHE-8340836 (C.E.S.).

Supplementary Material Available: Tables of anisotropic thermal parameters and bond distances and angles for the 200 K X-ray structure determination of $[Fe_3O(O_2CCH_3)_6(py)_3](py)$ (2 pages); listing of structure factor amplitudes (5 pages). Ordering information is given on any current masthead page.